Supplementary Information

**Thermally Responsive Spatially Programmable Soft Actuators with Multiple Response States Enabled by Grayscale UV Light Processing**

*Yizong Li, Sooyeon Noh Coodley, Si Chen, Penghao Dong, Su Li, Shanshan Yao**

## Estimation of Work Capacity

As shown in Fig. S13, the strain can be represented as:[1, 2]

$$\varepsilon = kt = \frac{2ht}{L^2 + h^2} \qquad \text{* MERGEFORMAT (S1)}$$

where $k$ denotes the curvature of the SPSA, $t$ represents the thickness of the SPSA, $L$ is half the length of the SPSA, and $h$ indicates the displacement at the SPSA's end. For SPSAs with BP-PDMS layers treated by photomasks of varying grayscale levels (Fig. S10), the corresponding strain values are 1.58%, 1.76%, 1.92%, 2.00%, 2.08%, and 2.15%.

The passive layer, BP-PDMS and gPDMS, act as structural constraints that influence the bending curvature of the SPSA, however, their contribution to energy density is minimal.[2] Therefore, only the active layer, LCE, is considered in the energy density calculation. The energy density is calculated as:

$$W = \frac{\sigma\varepsilon}{2} = \frac{E\varepsilon^2}{2} \qquad \text{* MERGEFORMAT (S2)}$$

where $\sigma$ is the actuation stress of the LCE layer, and E is Young's modulus of the LCE (2.83 MPa). Accordingly, the energy densities for SPSAs in Fig. S10 are calculated as 354.01, 437.46, 519.33, 568.32, 612.09, and 656.43 J/m$^3$

The work capacity is then given by:

$$W_{cap} = WV = \frac{E\varepsilon^2}{2} V \qquad \text{* MERGEFORMAT (S3)}$$

where $V$ is the volume of the LCE layer. The resulting work capacities for SPSAs in Fig. S10 are 7.97, 9.84, 11.69, 12.79, 13.77, and 14.77 µJ.

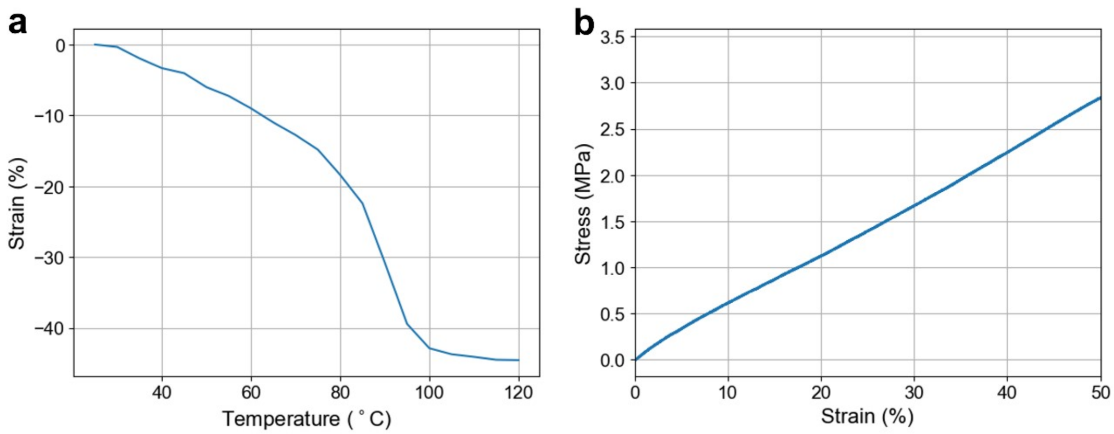


**Fig. S1. Mechanical properties of the LCE layer.** (a) The strain of the LCE layer as a function of temperature. (b) The stress-strain curve of the LCE layer at room temperature.

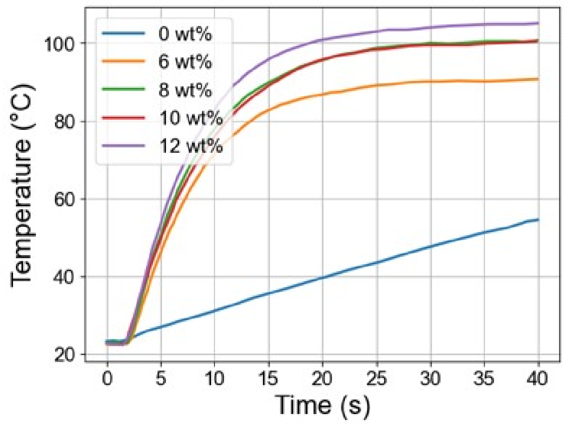


**Fig. S2. Temperature changes of gPDMS layers with varying graphite weight ratios under nIR light heating.** The gPDMS layer was positioned 10 cm below the nIR light source.

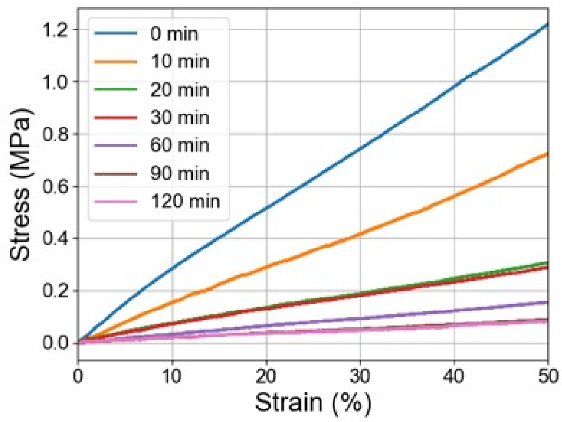


**Fig. S3. Stress-strain curves of BP-PDMS layers under different UV exposure times.** UV treatments were performed with a fully transparent photomask (grayscale 100%) at an intensity of 1.95 mW · $cm^{-2}$.

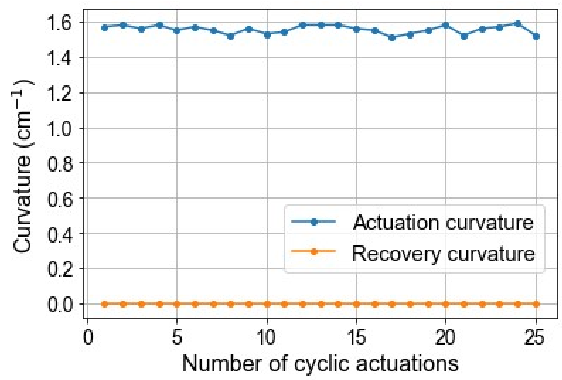


**Fig. S4. Cyclic actuation test.** The bonding between each layer of the SPSA remains robust after 25 cycles of actuation.

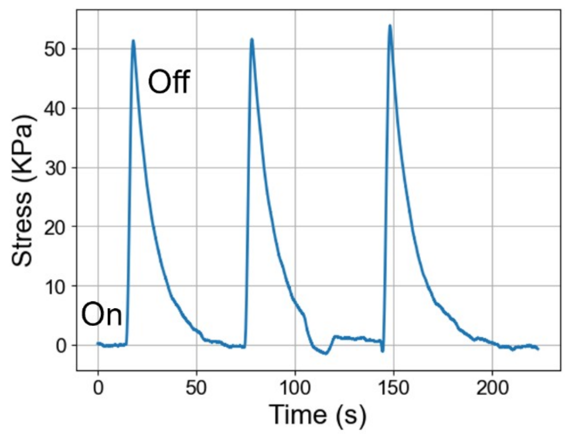


**Fig. S5. Characterization of the actuation stress.** The actuation stress of SPSA can reach up to 53 KPa.

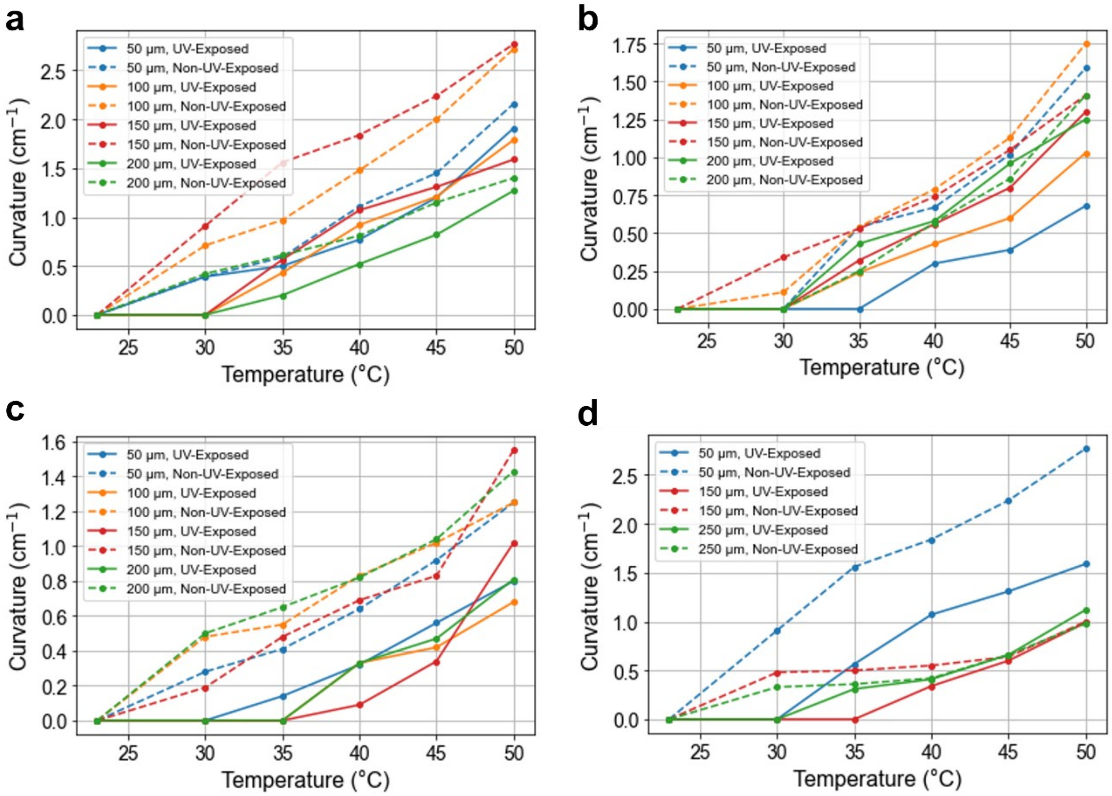


**Fig. S6. Comparisons of the curvature between SPSAs with the UV-exposed (solid line) and non-UV-exposed (dashed line) BP-PDMS.** (a-c) Curvatures as a function of temperature for a gPDMS layer thickness of 50 μm and BP-PDMS layer thicknesses ranging from 50 to 200 μm, with LCE layer thicknesses of (a) 150 μm, (b) 300 μm, and (c) 450 μm. (d) Curvatures as a function of temperature for BP-PDMS and LCE layer thicknesses of 150 μm, and gPDMS layer thicknesses ranging from 50 to 250 μm.

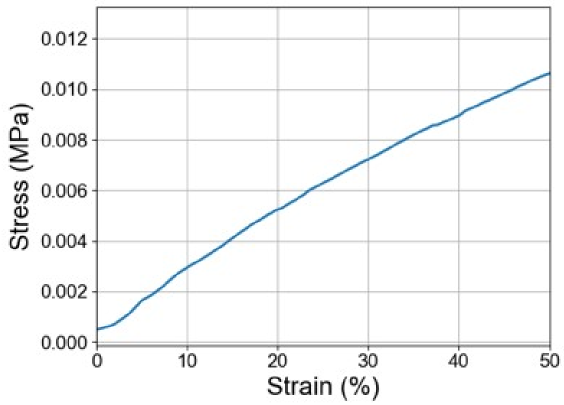


**Fig. S7. Stress-strain curve of the gPDMS layer.** The graphite loading ratio is 12 wt%.

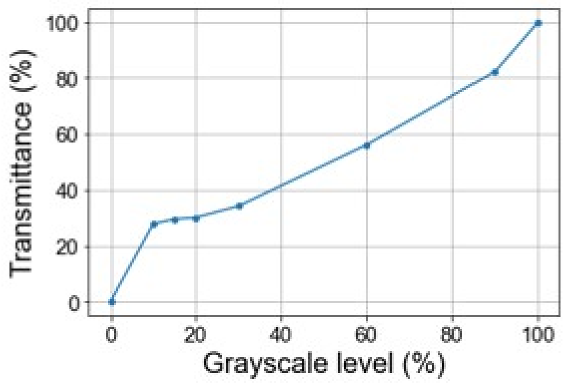


**Fig. S8. Transmittance of the photomask to the 365 nm UV light as a function of grayscale levels.**

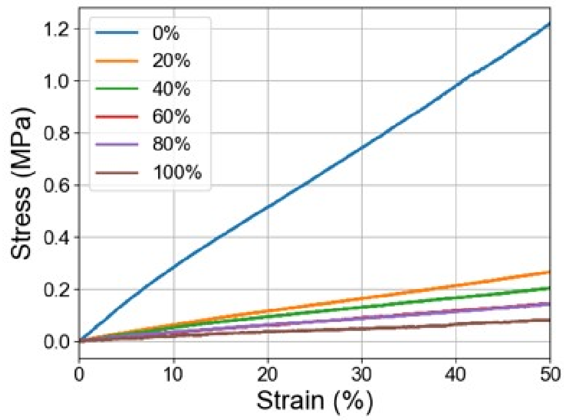


**Fig. S9. Stress-strain curves of the BP-PDMS layer made with photomasks of different grayscale levels**. The UV exposure time and intensity are maintained at 120 mins and 1.95 mW·cm$^{-2}$, respectively.

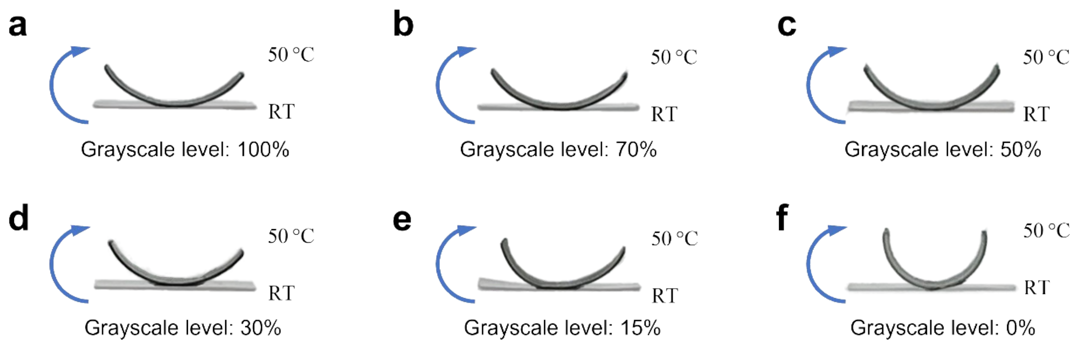


**Fig. S10. Snapshots of the thermal actuator when heated to 50 °C with BP-PDMS layers treated by photomasks of varying grayscale levels**: (a) 100%, (b) 70%, (c) 50%, (d) 30%, (e) 15%, and (f) 0%.

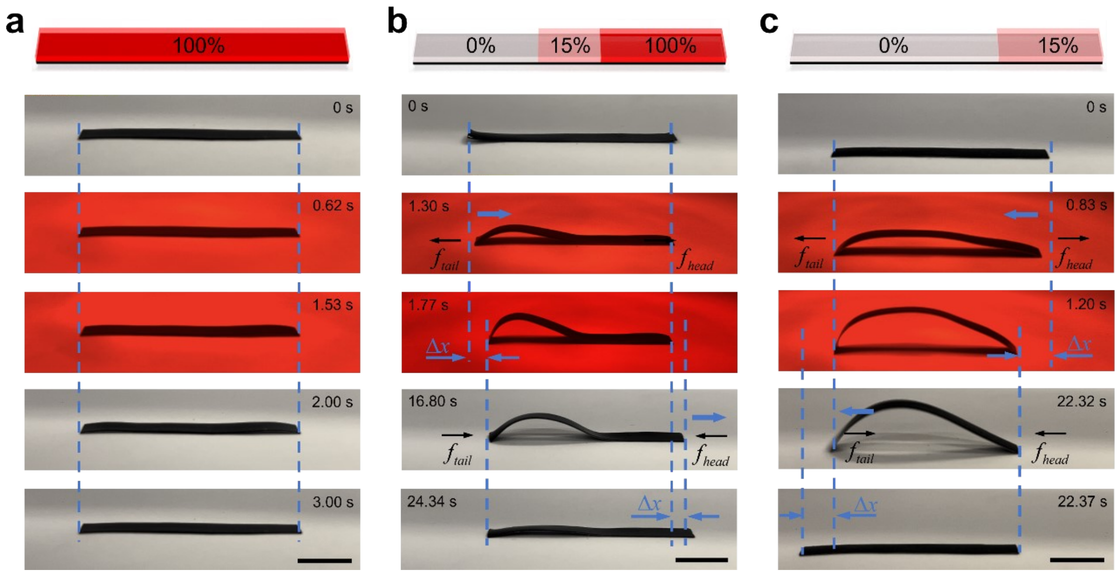


**Fig. S11. Influence of BP-PDMS pattern variations on the locomotion mode of caterpillar-inspired soft crawling robots.** (a) Soft robot with an intact-only pattern demonstrates intact actuation without directional locomotion. (b) Soft robot with a joint-to-intact length ratio of 3:1 exhibits forward locomotion. (c) Soft robot without an intact section displays backward locomotion. Combined with the pattern in Fig. 6c, we conclude that the joint-to-intact length ratio determines the locomotion mode: a 0:1 ratio results in intact deformation, 1:1 and 2:1 ratios enable forward locomotion, and 3:1 and 1:0 ratios produce backward locomotion. Scale bars: 10 mm.

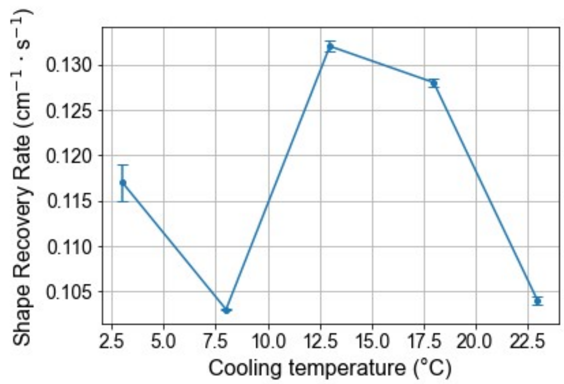


**Fig. S12. Effect of recovery temperatures on the shape recovery rate, measured from 3 °C to room temperature in 5 °C increments.**

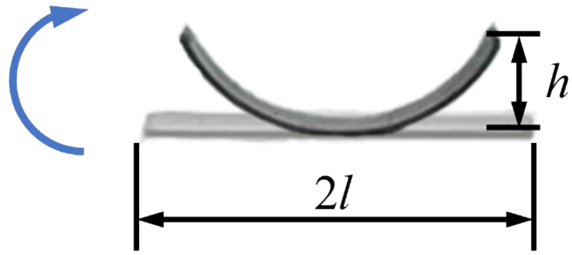


**Fig. S13. Schematic representation of deformation parameters in the SPSA.**

**Table S1. Representative spatially programmable soft thermal actuators.**

| Materials | Programming Mechanism | Untethered Actuation | Actuation Temperature (ºC) | Programmability | Curvature ($cm^{-1}$) | References |
|---|---|---|---|---|---|---|
| BP-PDMS/gPDMS/LCE | Material properties (Young's modulus by grayscale photomask) | ✓ | 30 or 50 | Multiple States | 0 – 2.77 | This work |
| LCE | Material properties (Decrosslinking of LCE by photomask) | ✓ | 70 | Multiple States | – | [3] |
| LCE | Material properties (Crosslinking of LCE by photomask) | ✓ | 65 | Binary States | – | [4] |
| LCE | Material properties (Crosslinking of LCE along lateral direction by photomask) | ✓ | 80 | Binary States | – | [5] |
| LCE | Material properties (Alignment of LCE) | ✓ | 175 | Binary States | – | [6] |
| LCE | Material properties (Crosslinking along lateral direction of LCE by photomask) | ✓ | 180 | Binary States | – | [7] |
| LCE | Material properties (Gradient crosslinking along thickness direction of LCE by photomask) | ✓ | 130 | Binary States | – | [8] |
| LCE | Material properties (Gradient crosslinking along thickness direction of LCE by photomask) | ✓ | 80 | Binary States | – | [9] |
| Polyimide/PDMS/AgNW | Geometreis (Thickness and layout of polyimide or AgNW) | ✗ | 160 | Multiple States | 0 – 2.6 | [10] |
| Polyester/paper | Geometreis (Thickness of polyester) | ✓ | 90 | Multiple States | 0.7 – 1.8 | [11] |
| LCN/GO | Geometreis (Selective deposition of GO layer) | ✓ | -- | Binary States | -0.35 or 0.28 | [12] |

| | | | | | | |
|---|---|---|---|---|---|---|
| Mxene/Polycarbonate | Geometreis (Selective deposition of Mxene) | ✓ | 80 | Binary States | – | [13] |
| Superaligned CNT array/PDMS | Geometries (Angle between current direction and CNT alignment direction) | ✗ | 125 | Multiple States | 0 – 0.77 | [14] |
| LCE | Geometries (Relative position between two LCE layers) | ✓ | 92 and 127 | Binary States | – | [15] |
| LDPE/AgNW/PVC | Geometreis (Angle between longitudinal direction of the LDPE film and the actuator) | ✗ | 40 | Binary States | 0 or 2.5 | [16] |

[a)] BP-PDMS = benzophenone-poly(dimethylsiloxane), gPDMS = graphite-PDMS, LCE = liquid crystal elastomer, LDPE = low density polyethylene, AgNW = silver nanowire, PVC = polyvinyl chloride, LCN = liquid crystal network, GO = graphene oxide, CNT = carbon nanotube

References


1. T. Sugino, K. Kiyohara, I. Takeuchi, K. Mukai and K. Asaka, *Sens. Actuat. B-CHEM.*, 2009, **141**, 179-186.
2. C. Lu, Y. Yang, J. Wang, R. Fu, X. Zhao, L. Zhao, Y. Ming, Y. Hu, H. Lin and X. Tao, *Nat. Commun.*, 2018, **9**, 752.
3. Z. C. Jiang, Y. Y. Xiao, X. Tong and Y. Zhao, *Angew. Chem. Int. Ed.*, 2019, **131**, 5386.
4. R. Yang and Y. Zhao, *Angew. Chem. Int. Ed.*, 2017, **129**, 14390.
5. B. Jin, H. Song, R. Jiang, J. Song, Q. Zhao and T. Xie, *Sci. Adv.*, 2018, **4**, eaao3865.
6. T. H. Ware, M. E. McConney, J. J. Wie, V. P. Tondiglia and T. J. White, *Science*, 2015, **347**, 982.
7. T. S. Hebner, R. G. Bowman, D. Duffy, C. Mostajeran, I. Griniasty, I. Cohen, M. Warner, C. N. Bowman and T. J. White, *ACS Appl. Mater. Interfaces*, 2023, **15**, 11092-11098.
8. J. Hu, Z.-Y. Kuang, L. Tao, Y.-F. Huang, Q. Wang, H.-L. Xie, J.-R. Yin and E.-Q. Chen, *ACS Appl. Mater. Interfaces*, 2019, **11**, 48393-48401.
9. D. Sezen Polat, V. E. Buurman, D. J. Mulder and D. Liu, *Chem. Eur. J.*, 2024, **30**, e202400515.
10. S. Yao, J. Cui, Z. Cui and Y. Zhu, *Nanoscale*, 2017, **9**, 3797.
11. X. Li, Y. Du, C. Xiao, X. Ding, X. Pan, K. Zheng, X. Liu, L. Chen, Y. Gong and M. Xue, *Adv. Funct. Mater.*, 2023, **34**, 2310380.
12. L. Zhang, J. Pan, Y. Liu, Y. Xu and A. Zhang, *ACS Appl. Mater. Interfaces*, 2020, **12**, 6727-6735.
13. G. Cai, J.-H. Ciou, Y. Liu, Y. Jiang and P. S. Lee, *Sci. Adv.*, 2019, **5**, eaaw7956.
14. Q. Li, C. Liu, Y.-H. Lin, L. Liu, K. Jiang and S. Fan, *ACS Nano*, 2015, **9**, 409-418.
15. A. Kotikian, C. McMahan, E. C. Davidson, J. M. Muhammad, R. D. Weeks, C. Daraio and J. A. Lewis, *Sci. Robot.*, 2019, **4**, eaax7044.
16. H. Kim, H. Lee, I. Ha, J. Jung, P. Won, H. Cho, J. Yeo, S. Hong, S. Han and J. Kwon, *Adv. Funct. Mater.*, 2018, **28**, 1801847.